

## Body Height Estimation System Based on Binocular Vision

<https://doi.org/10.3991/ijoe.v14i04.8400>

Guangyi Yang, Deshi Li, Guobao Ru<sup>(✉)</sup>, Jiahua Cao, Weizheng Jin  
Wuhan University, Wuhan, China  
rgb@whu.edu.cn

**Abstract**—In this paper, we propose a novel approach to estimate body height from video sequences based on binocular stereo vision. Firstly, we built a parallel binocular stereo vision device and detected the foreground by using Gaussian mixture model. After shadow elimination, we proposed the contour screening algorithm to obtain the human foreground and the top point in the foreground image. Then, we detected SURF feature points in the binocular images and screened them for 3 times to calculate the disparity of the head. After that, the height of human bodies can be estimated with the calibration parameters of binocular cameras. The experimental results demonstrate that the proposed method has higher measurement accuracy and spends less time which proves the effectiveness of the method.

**Keywords**—binocular vision, height measurement, human body, Gaussian mixture model, feature matching.

### 1 Introduction

Body height is an important part of the human body's 3D information. In daily life, height measurement is one of the basic items of the physical examination. In some ticketing system (for example scenic spot tickets, train tickets), height measurement is also necessary to determine every customer's ticket price.

Currently, height measurement is mainly based on the contact measuring method which obtains the length from the top of head to the sole of feet with a measuring tool. It has a high precision and little requirement of measurement environment. However, the full cooperation is needed from the person being measured which would take lots of time. Nowadays, machine vision photogrammetry, as a major research direction in the non-contact 3D measurement technology, is mainly divided into monocular vision and binocular vision [1-11]. Reference [1] extracts human foreground with the Codebook model, estimates the vanishing line of the ground plane and the vertical vanishing point [2] to calculate the body height using the cross ratio invariance. But this method requires a known height of a reference object. Reference [3] combines projective geometry with single-view metrology and proposes a statistical method in the Bayesian-like framework without using reference length in the image plane. However, it's strict with the body position and the human feature points need

to be extracted manually from a single image. Reference [4] obtains the head and feet feature points using the vertical vanishing point and constructs several constraint equations to estimate the perpendicular point, then estimates the body height. Nevertheless, there are some errors with the proposed constraint equations. Reference [6] takes the ratios of features in the human face into account to estimate the stature of human body. But this method can only estimate the stature roughly. Reference [7] proposes a pedestrian height measurement method based on binocular vision. The 3D coordinates of the points are calculated with the background difference and the disparity map is based on ELAS algorithm. The human feature points are tracked with the target track algorithm to get the stable value of the stature. Reference [9] utilizes the depth camera of Kinect based on the light coding technology to obtain the disparity map of the current scene, then restores the stature of the human body in the image. However, this method relies on the support of the Kinect.

In order to estimate the body height fast and accurately, we propose a new method of body height estimation based on binocular stereo vision. Firstly, subtract the background information from the scene using background modeling. After shadow elimination and contour screening, we get the human foreground and the coordinate of top of the head. Then, we detect SURF feature points in binocular images and screen out correct matching points in the human foreground to calculate the head disparity. Finally, the body height can be obtained with the results of camera calibration, the coordinate of top of the head and the head disparity.

The rest of this paper is organized as follows. In Section 2, we introduce the mathematical model of binocular stereo vision and propose the overall measurement scheme of body height. Then, we discuss every step of the scheme in detail. In Section 3, we provide a brief introduction to Gaussian mixture model used in the foreground extraction and propose the contour screening algorithm to obtain the human foreground and top points. After that, in order to estimate the disparity of top points, we introduce the SURF algorithm and describe how to screen feature points to calculate the head disparity in Section 4. In Section 5, we discuss the calculation of body height. Finally, the experimental results are given in Section 6 and conclusions are drawn in Section 7.

## 2 The Measurement Scheme of Stature

### 2.1 The Mathematical Model of Binocular Stereo Vision

As shown in Figure 1, the system uses parallel binocular vision to restore the 3D information of top of the head, thereby estimating the body height. In order to facilitate the subsequent estimation of the body height, we choose the left camera coordinate system as the world coordinate system of binocular vision system. The intrinsic parameters of the left and right cameras (such as focal length, the coordinate of principle point and the distortion coefficients) are obtained with the Zhang's camera calibration method [12]. Then, compute the geometrical relationship between the two cameras in space (rotation matrix  $R$  and translation vector  $T$ ). Finally, the binocular

images are rectified with Bouguet rectification method [17] to make sure the image rows between the two cameras to be aligned after rectification.

According to geometric projection relations, we can get the correspondence between 2D projection points  $(x_l, y_l)$  in the left camera’s image pixel coordinate system and 3D points  $(X_w, Y_w, Z_w)$  in the world coordinate system as follows.

$$\begin{cases} X_w = \frac{(x_l - c_x) \times T_x}{-d} \\ Y_w = \frac{(y_l - c_y) \times T_x}{-d} \\ Z_w = \frac{f \times T_x}{-d} \end{cases} \quad (1)$$

Where  $f$  is the focal length of the left camera,  $(c_x, c_y)$  is the coordinate of the principle point in the left camera’s image pixel coordinate system,  $T_x$  is the baseline length of the binocular cameras,  $d$  is the disparity of matching points. Here we define top of the head in the left image as the top point  $p_{top}(x_{top}, y_{top})$ . For  $p_{top}$ , we need to estimate the corresponding disparity  $Disp_{top}$  to restore its 3D information. The system uses feature matching to obtain the matching points which are the closest to  $p_{top}$ . Then, calculate the disparity of the matching points  $Disp_{head}$  to estimate the disparity of the top point  $Disp_{top}$ .

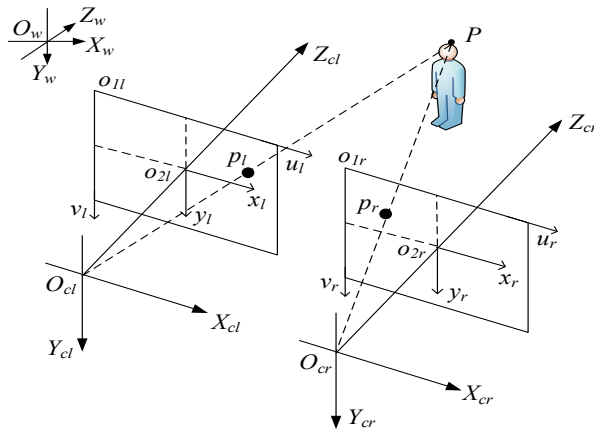


Fig. 1. The imaging model of the binocular stereo vision

## 2.2 The Measurement Process

As shown in Figure 2, it’s the flowchart of measuring the height of human body.

1. Setting up a parallel binocular stereo vision system: fix binocular cameras on the tripods with a pan-and-tilt and make sure that binocular cameras are perpendicular to the horizontal ground. Adjust focal length, RGB gain, contrast ratio and exposure parameters of binocular cameras to the same.

2. Calibrating the binocular cameras: Firstly, the intrinsic and extrinsic parameters of binocular cameras are obtained after the Zhang’s single camera calibration [12] and stereo calibration. Then, the image rows between two cameras are rectified to be aligned with Bouguet rectification algorithm [17].
3. Extracting human foreground and the top point’s coordinate: detect moving foreground in the video sequence of binocular cameras by using Gaussian mixture model [13-15], eliminate shadow and screen out the largest human contour. After that, extract the coordinate of top point.
4. Feature matching in the area of human foreground: the feature points of left-and-right images are detected by SURF algorithm [18]. Then, the SURF feature points are screened for 3 times to obtain matching points in the human foreground and We select matching points which are the closest to the top points to calculate the disparity of head.
5. Calculating the height of human body: estimate the relative height of the top point with calibration parameters, the coordinate of the top point and the disparity of head. After linear correction, the relative height and the vertical height of binocular cameras make the height of human body.

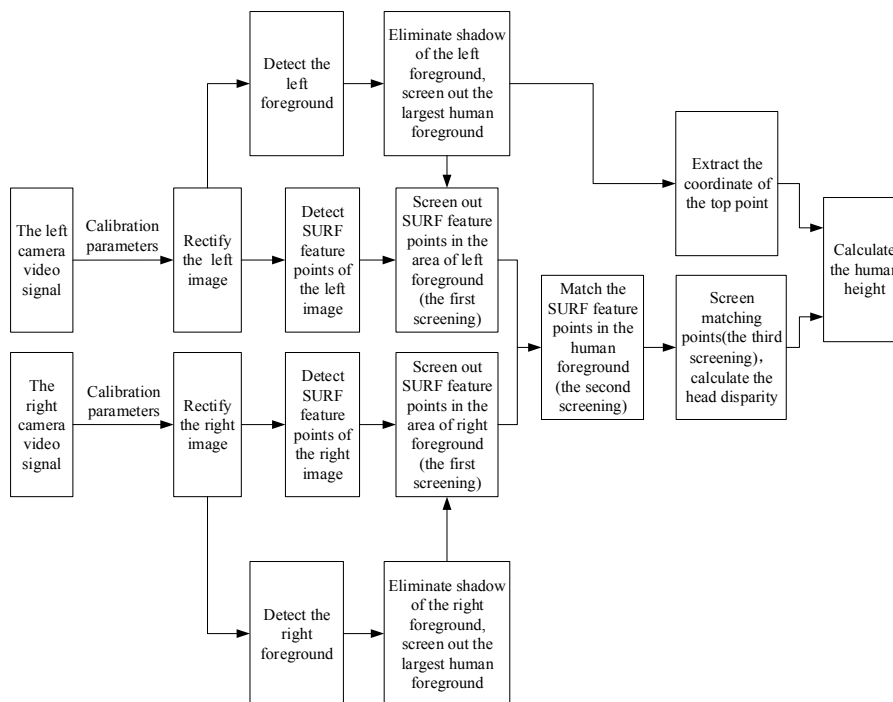


Fig. 2. The flowchart of measuring the body height

### 3 The Human Foreground and the Top Point Extraction

The body height estimation system uses Gaussian mixture model [13-15] to do the moving foreground segmentation in the video sequence of binocular cameras. After shadow elimination and contour screening, body silhouettes and the coordinates of top points can be extracted from the binocular images.

#### 3.1 Gaussian Mixture Model

Every pixel in images of video sequences is modeled by a mixture of  $K$  Gaussian distributions. In general, the value of  $K$  ranges from 3 to 5 in order to make the model adaptive to the lighting changes and scene changes.  $I_{t,xy} = [R_{t,xy}, G_{t,xy}, B_{t,xy}]^T$  is a particular pixel at time  $t$ . The probability of observing  $I_{t,xy}$  is

$$f(I_{t,xy}) = \sum_{i=1}^K \omega_{i,t,xy} \times \eta(I_{t,xy} | \mu_{i,t,xy}, \Sigma_{i,t,xy}) \quad (2)$$

Where  $\omega_{i,t,xy}$  is the weight parameter of the  $i^{\text{th}}$  Gaussian distribution at time  $t$ ,  $\eta(I_{t,xy} | \mu_{i,t,xy}, \Sigma_{i,t,xy})$  is the  $i^{\text{th}}$  Gaussian probability density function at time  $t$ , its mean value and covariance matrix are  $\mu_{i,t,xy}$  and  $\Sigma_{i,t,xy}$ . Assuming that 3 channels of RGB images are independent to each other, the covariance matrix can be expressed as  $\Sigma_{i,t,xy} = \sigma_{i,t,xy}^2 I$ .  $\sigma_{i,t,xy}^2$  is the variance of the  $i^{\text{th}}$  Gaussian distribution.

**Model parameters initialization.** Firstly, the mean value of the 1<sup>st</sup> Gaussian distribution is initialized with the RGB value of all pixels in the first frame. Then, initialize  $K$  Gaussian distributions with the same weight and a high variance  $varInit$  as follows.

$$\omega_{i,0,xy} = \frac{1}{K} \quad (3)$$

$$\sigma_{i,0,xy}^2 = varInit \quad (4)$$

**Updating model parameters.** Every pixel in the next frame image need to be checked against the existing  $K$  Gaussian distributions, until a match is found. A match is defined as a pixel value within 2.5 standard deviations of a distribution as Formula 5.

$$|I_{t,xy} - \mu_{i,t-1,xy}| \leq 2.5\sigma_{i,t-1,xy} \quad (5)$$

Where  $\sigma_{i,t-1,xy}$  is the standard deviation of the  $i^{\text{th}}$  Gaussian distribution. According to whether the match is found, the  $K$  Gaussian distributions are updated as Formula 6.

$$\begin{cases} \omega_{i,t,xy} = \omega_{i,t-1,xy} + \alpha(M - \omega_{i,t-1,xy}) \\ \mu_{i,t,xy} = \mu_{i,t-1,xy} + M \left( \frac{\alpha}{\omega_{i,t,xy}} \right) (I_{t,xy} - \mu_{i,t-1,xy}) \\ \sigma_{i,t,xy}^2 = \sigma_{i,t-1,xy}^2 + M \left( \frac{\alpha}{\omega_{i,t,xy}} \right) [(I_{t,xy} - \mu_{i,t-1,xy})^2 - \sigma_{i,t-1,xy}^2] \end{cases} \quad (6)$$

Where  $\alpha$  is the learning rate which ranges from 0 to 1. The higher  $\alpha$  is, the faster the model is updated.  $M$  is 1 for the model which matched and 0 for the remaining models. If none of the  $K$  Gaussian distributions match current pixel value, a new Gaussian distribution would be generated to replace the  $n^{\text{th}}$  distribution which is the least probable. The parameters of the new Gaussian distribution is as Formula 7.

$$\begin{cases} \omega_{n,t,xy} = \alpha \\ \mu_{n,t,xy} = I_{t,xy} \\ \sigma_{n,t,xy}^2 = varInit \end{cases} \quad (7)$$

Renormalize the weights of the  $K$  Gaussian distributions after updating the model. Then, order  $K$  Gaussian distributions by the value  $\frac{\omega_{i,t,xy}}{\sigma_{i,t,xy}}$ .

**Background estimation.** As shown in Formula 8, the first  $B$  distributions are chosen as the background model and others model the foreground.

$$B = \arg \min_b (\sum_{i=1}^b \omega_{i,t,xy} > 1 - c_f) \quad (8)$$

Where  $1 - c_f$  is a pre-set threshold.  $c_f$  is a measure of the maximum portion of the data that can belong to pixels without influencing the background model. If matching one of the first  $B$  distributions, the current pixel value is regarded as a background pixel, otherwise as a foreground pixel.

### 3.2 Human Foreground Image Processing and Coordinates Extraction

After the human foreground image is extracted, the color distortion and brightness distortion are estimated to detect and eliminate the shadow of the human foreground according to the shadow detection model proposed in Reference [16]. Considering that the system only estimate a single body at one time, we propose the contour screening algorithm to calculate the area of all contours in the foreground image and only retain the largest connected domain as the human foreground. It's an efficient way to prevent the interference from image noise. The contour screening algorithm is presented as follows.

---

**Algorithm** Contour Screening Algorithm

---

**Initialization:**

```

Set seqCount = 0, arearMaxContour = NULL,
   contourAreaMax = 0, contourAreaTemp = 0
1: count numSeq
2: while seqCount < numSeq do
3:   Return a Seq
4:   Calculate contourAreaTemp
5:   if contourAreaTemp > contourAreaMax then
6:     areaMaxContour=Seq
7:     contourAreaMax=contourAreaTemp
8:   else
9:     deleteSeq
10:  end if
11:  seqCount++
12: end while

```

---

In the contour screening algorithm,  $numSeq$  is the amount of all contours in the foreground image.  $areaMaxContour$  denotes the largest contour and  $contourAreaMax$  denotes the maximum area value.  $contourAreaTemp$  is the temporary variable of the area and  $Seq$  denotes one of contours in the foreground image. We calculate the area of all contours to obtain the largest connected domain in the foreground image. During the measurement, the largest connected domain is just the human foreground. Deleting smaller connected domains could prevent the human foreground from the image noise.



Fig. 3. Human foreground and the top point extraction

After we obtain the human foreground and contour, go through coordinates of human contour and take the point which has the minimum  $v$  coordinate as the top point  $p_{top}(x_{top}, y_{top})$ . We use bounding boxes and circles(gray values are 125) to mark boundaries and top points. Human foreground image and the top point extraction are shown in Figure 3.

## 4 Feature Matching in the Human Foreground

In order to calculate the head disparity  $Disp_{head}$ , the system firstly detects the SURF feature points in binocular images and screens all feature points for 3 times to obtain correct feature matching points in the head of human foreground. Then, we can estimate the head disparity.

### 4.1 SURF Feature Point Detection

SURF [18] is a speeded-up feature robust algorithm based on SIFT [19]. SURF feature points are invariant to image scaling, translation and rotation, and partially invariant to illumination change. What's more, SURF is not only highly robust, but much faster than SIFT. SURF algorithm mainly consists of feature points detection, orientation assignment, feature points description.

**Feature points detection.** SURF algorithm is based on the Hessian matrix. The discriminant of the matrix can roughly screens the location of interest points in the image. Given a point  $X(x,y)$  in an image  $I$ , the Hessian matrix  $H(X, \sigma)$  in  $X$  at scale  $\sigma$  is defined as follows.

$$H(X, \sigma) = \begin{bmatrix} L_{xx}(X, \sigma) & L_{xy}(X, \sigma) \\ L_{xy}(X, \sigma) & L_{yy}(X, \sigma) \end{bmatrix} \quad (9)$$

Where  $L_{xx}(X, \sigma)$  is the convolution of the Gaussian second order derivative  $\frac{\partial^2}{\partial x^2} G(x, y, \sigma)$  with the image  $I$  in point  $X$  and similarly for  $L_{xy}(X, \sigma)$  and  $L_{yy}(X, \sigma)$ . As shown in Figure 4, SURF algorithm makes use of integral image and box filter to approximate the Gaussian second order derivative for speeding up the calculation of the convolution. The approximations are denoted as  $D_{xx}$ ,  $D_{xy}$ ,  $D_{yy}$ . SURF algorithm proposes Formula 10 as the determinant of the Hessian matrix.

$$\det(H_{approx}) = D_{xx}D_{yy} - (0.9D_{xy})^2 \quad (10)$$

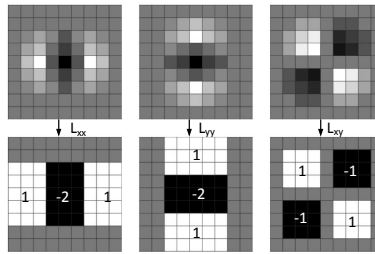


Fig. 4. Laplacian of Gaussian approximation with box filters

SURF keeps the size of the input image constant and upscales the size of box filters to construct the image pyramid. The initial scale layer of the image pyramid is the convolution of the original image and the  $9 \times 9$  box filters which correspond to scale  $\sigma = 1.2$ . Subsequent layers are obtained by filtering the original image with the box filters the size of which gradually becomes bigger. In order to maintain the structure of box filters, the smallest step size of two consecutive box filters must be 6.

According to Formula 10, the local extremum could be detected as an interest point. Then, a non-maximum suppression is applied in the scale space to compare the interest point with its 26 neighbours and only the maximum and minima can be regarded as the feature point. Finally, interpolate the nearby data of the feature point in the scale space to find the location to subpixel accuracy.

**Orientation assignment.** After locating all feature points, SURF calculates the Haar wavelet responses of size  $4\sigma$  within a radius of  $6\sigma$  of the feature point. Furthermore, the responses are weighted with the Gaussian the standard deviation of which is  $2.5\sigma$ . Rotate a circular sector covering an angle of  $\frac{\pi}{3}$  to calculate the sum of the Haar wavelet responses around the origin and choose the longest vector as the orientation of the feature point.

**The description of the feature point.** After assigning the orientation of the feature points, SURF constructs a square window the orientation of which is the same with the direction of the feature points. The window the size of which is  $20\sigma$  is divided into  $4 \times 4$  subregions. Calculate the Haar wavelet responses of each subregion.  $dx$  de-

notes the Haar wavelet response in horizontal direction and  $dy$  denotes the Haar wavelet response in vertical direction. The responses need to be weighted with an  $(3.3\sigma)$ . Then, in each subregions,  $dx$ ,  $dy$  and the absolute values  $|dx|$ ,  $|dy|$  are summed up to form a four-dimensional descriptor vector as follows.

$$v = [\Sigma dx, \Sigma dy, \Sigma |dx|, \Sigma |dy|] \tag{11}$$

There are  $4 \times 4$  subregions for each feature point which results in a descriptor vector of length 64.

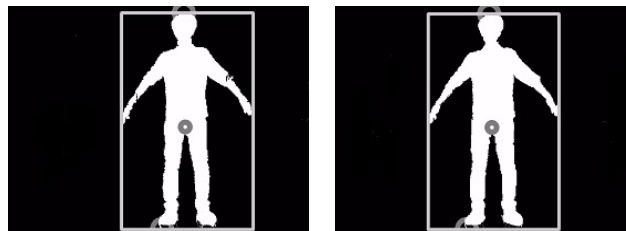
#### 4.2 Three Times Screening of the Feature Points

In the actual measurement of body height, we only want to get matching points in the human foreground and calculate the head disparity. Therefore, it's necessary to screen out correct matching points from all detected feature points.

**The first screening.** The system uses white pixels (gray values are 255) to mark the foreground region, while using black pixels (gray values are 0) to mark the background region. Then, the system can determine whether the feature point belongs to the foreground by the gray value of its coordinate in the foreground image. Set the coordinate of the feature point as  $X(x_k, y_k)$ , and  $gvf(x_k, y_k)$  denotes the gray value of the feature point's coordinate in the foreground image. If  $gvf(x_k, y_k) = 255$ ,  $X(x_k, y_k)$  belongs to the foreground region and we retain the feature point; if  $gvf(x_k, y_k) \neq 255$ ,  $X(x_k, y_k)$  belongs to the background region, so we exclude the feature point. As shown in the following three sets of images, Figure 5(a) is the left and right view of the original feature point images before screening, Figure 5(b) is the extracted foreground image of the corresponding frame from the scene, Figure 5(c) is the feature point images after the first screening.



(a) The original feature points image before the first screening



(b) The extracted human foreground of the corresponding frame



(c) The feature points image after the first screening

**Fig. 5.** The first screening effect

As shown in Figure 5, taking the test images for example, 1819 SURF feature points are detected in the left original image, 1814 in the right original image. After the first screening, 243 feature points in the left human foreground and 231 feature points in the right human foreground are reserved.

**The second screening.** The second screening is the process of feature matching. The system takes an effective method of feature matching by comparing the Euclidean distance of the closest neighbor to that of the second-closest neighbor [19]. Set that  $P_{li}$  is the  $i^{\text{th}}$  feature point of the left image,  $P_{rj}$  is the  $j^{\text{th}}$  feature point of the right image, the descriptor vectors of these two feature point are  $Descr_{li}$  and  $Descr_{rj}$ . The Euclidean distance of these two feature point is defined as follows.

$$D(P_{li}, P_{rj}) = \sqrt{\sum_{k=1}^m (Descr_{li}^k - Descr_{rj}^k)^2} \quad (12)$$

Where  $m$  is the dimensions of the descriptor vector,  $Descr_{li}^k$  and  $Descr_{rj}^k$  are respectively the  $k^{\text{th}}$  element of the descriptor vector of  $P_{li}$  and  $P_{rj}$ . Set that  $ND$  is the closest distance,  $NND$  is the second closest distance. The ratio of distances is defined as  $Ratio = \frac{ND}{NND}$ ,  $\omega$  is set as the threshold. Only when  $Ratio \leq \omega$  can the match be considered reliable, otherwise unreliable. The principle of the matching method is that we only match two feature points when  $ND$  is much smaller than  $NND$  which can lower the false matching rate effectively. In the experiment, we set  $\omega$  as 0.6. The second screening effect is shown in Figure 6.



**Fig. 6.** The second screening effect

As shown in Figure 6, after the second screening, there are 49 matching points left which still contain error matching points.

**The third screening.** The system is based on the parallel binocular stereo vision. Therefore, after stereo rectification, the binocular images should reside in the same plane with image rows aligned into a frontal parallel configuration. Taking the error of the stereo rectification into account, the absolute value of the  $v$ -axis coordinate difference between a pair of matching points should be 0 or few pixels unit which we define as  $dv = |y_{kl} - y_{kr}|$ .  $X_{kl}(x_{kl}, y_{kl})$  and  $X_{kr}(x_{kr}, y_{kr})$  denote the coordinates of the matching points after the second screening and  $vThresh$  denotes the screening threshold of the matching points. If  $dv < vThresh$ , we retain the matching points; If  $dv \geq vThresh$ , we delete the matching points. In the experiment,  $vThresh$  is equal to 2. The third screening effect is shown in Figure 7.



Fig. 7. The third screening effect

As shown in Figure 7, after screening for 3 times, there are 45 matching points left. Compared with the second screening, the third screening eliminates 4 error matching points. It can be seen that screening for 3 times not only eliminates the matching points in the background region which we are not interested in, but greatly eliminates the error matching points in the human foreground region.

After feature matching in the human foreground, the system screens out the matching points which are the closest to the top of head  $p_{top}(x_{top}, y_{top})$  as the head matching points.  $p_{hl}(x_{hl}, y_{hl})$  and  $p_{hr}(x_{hr}, y_{hr})$  denote the matching points of the head. Then, the head disparity is:

$$Disp_{head} = |x_{hr} - x_{hl}| \quad (13)$$

## 5 The Calculation of Body Height

According to Formula 1, the coordinate of the top point in the world coordinate system (the left camera coordinate system) can be restored with the calibration parameters, the coordinate of  $p_{top}(x_{top}, y_{top})$  and the head disparity  $Disp_{head}$ . Because the system is used to measure the body height, we only concern about the  $Y_w$ -axis coordinate values  $Y_{man}$  which is

$$Y_{man} = \frac{(y_{top} - c_y) \times T_x}{-Disp_{head}} \quad (14)$$

Ideally, the  $Y_w$ -axis of the world coordinate system is vertical to the horizontal ground. Therefore, the body height  $H_{man}$  is

$$H_{man} = |Y_{man}| + H_c \tag{15}$$

Where  $H_c$  is the vertical height of the binocular cameras. In fact, it's difficult to make the  $Y_w$ -axis vertical to the horizontal ground perfectly. Hence, we need to correct  $Y_{man}$  linealy before using Formula 15 to caculate the body height.

## 6 Experiment Results and Analysis

We do the experiment indoor where the illumination is stable and the floor is flat. In the experiment,  $|Y_{man}'|$  denotes the vertical height between top of the head and the origin of the left camera coordinate system. Firstly we take 9 people whose body height we already know to linearly fit  $|Y_{man}|$  and  $|Y_{man}'|$ . After obtaining fitting parameters, the system can linearly corrects  $|Y_{man}|$  and estimate the body height. Here we take another 10 people at random to estimate their body height. The experiment is based on Window7 operating system, using Visual Studio 2013 and OpenCV 2.4.9 as software platforms. The computer processor is Intel Core i7-3520M, clocked at 2.90 GHz. The resolution of the test video is 640\*480. The camera model is SUNTIME 300C from Taiwan. The mapping table of  $|Y_{man}|$  and  $|Y_{man}'|$  is shown in Table 1.

**Table 1.** Mapping table of  $|Y_{man}|$  and  $|Y_{man}'|$

No.	$ Y_{man} $ (mm)	$ Y_{man}' $ (mm)	No.	$ Y_{man} $ (mm)	$ Y_{man}' $ (mm)
1	971	1053	6	1043	1115
2	890	990	7	969	1064
3	924	1020	8	755	855
4	948	1025	9	842	935
5	857	945			

We linearly fit  $|Y_{man}|$  and  $|Y_{man}'|$  in the MATLAB to weaken the effect of the camera coordinate system which is not vertical to the horizontal ground perfectly and the systematic error. The linear fitting of  $|Y_{man}|$  and  $|Y_{man}'|$  is shown in Figure 8.

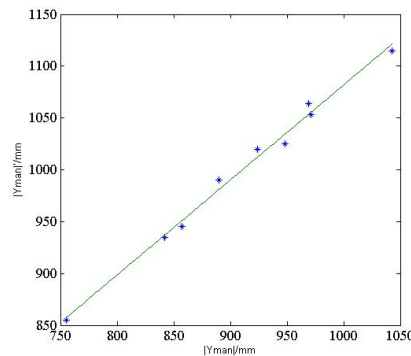


**Fig. 8.** The linear fitting of  $|Y_{man}|$  and  $|Y_{man}'|$

After linear fitting, the correspondence relationship of  $|Y_{man}|$  and  $|Y_{man}'|$  can be represented with a linear equation  $y = kx + b$ . In the experiment,  $k=0.9171$  and  $b=164.7176$ . Then, we linearly correct  $|Y_{man}|$  to get the value of  $|Y_{man}'|$ . As shown in Formula 15, the body height  $H_{man}$  can be estimated by  $H_{man} = |Y_{man}'| + H_c$ . In the experiment,  $H_c$  is set as 710 mm. Then, we make use of the system to estimate the body height of another 10 people and each was measured for three times. The measurement results are shown as Table 2.

**Table 2.** The measurement data of stature and error analysis

No.	H <sub>man</sub> (mm)	True height (mm)	AE (mm)	RE (%)	No.	H <sub>man</sub> (mm)	True height (mm)	AE (mm)	RE (%)
1	1805	1802	3	0.056	6	1628	1630	2	0.123
	1813	1802	11	0.610		1624	1630	6	0.368
	1796	1802	6	0.333		1616	1630	14	0.859
2	1720	1720	0	0.000	7	1708	1718	10	0.582
	1712	1720	8	0.465		1731	1718	13	0.757
	1728	1720	8	0.465		1709	1718	9	0.524
3	1713	1698	15	0.883	8	1741	1750	9	0.514
	1709	1698	11	0.648		1773	1750	23	1.314
	1689	1698	9	0.530		1763	1750	13	0.743
4	1661	1673	12	0.717	9	1584	1570	14	0.892
	1655	1673	18	1.076		1556	1570	14	0.892
	1653	1673	20	1.196		1568	1570	2	0.127
5	1702	1701	1	0.059	10	1859	1850	9	0.487
	1706	1701	5	0.294		1853	1850	3	0.162
	1677	1701	24	1.411		1852	1850	2	0.108

As shown in Table 2, in the experiment, the accuracy of measurements shows the high precision and the absolute error(AE) is within the range of 24mm, the relative error(RE) is within the range of 1.5%. The error is mainly from the disparity difference between  $Disp_{top}$  and  $Disp_{head}$  which are close to each other but not the same, because  $Disp_{head}$  depends on the SURF matching points in the human foreground and we use it to estimate the disparity of the top points  $Disp_{top}$ . What's more, the distance between human body and binocular cameras can also influence the accuracy. The farther human body stands, the less accurate the measurement is. In the experiment, the distance ranged from 3.6m to 4.6m. The difference among 3 measurements of every human body is within the range of 32mm, which shows the stability of the system. And It takes about 2s for each measurement. Overall, the system meets the basic measuring needs of the body height. The interface of body height estimation system is shown in Figure 9. The whole test video has been uploaded to the website <http://my.tv.sohu.com/us/301042037/84985757.shtml>.



Fig. 9. The interface of body height estimation system

## 7 Conclusion

In this paper, we propose a new kind of body height estimation system based on binocular vision. First, the system uses the Gaussian mixture model to extract the foreground. After shadow elimination and contour screening, the human foreground and the coordinate of the top point are obtained. Then we detect the SURF feature points in the binocular images and screen them for 3 times to calculate the head disparity. Combined with the calibration parameters, the body height can be estimated. Experiments show that the system has relatively good accuracy and stability. It also takes relatively short time for every measurement. The system meets the basic measuring needs of the body height in the stable measurement circumstances.

## 8 Acknowledgements

This paper is supported by the National Natural Science Foundation of China (NSFC) (No. 61671333, 61571334).

## 9 References

- [1] M. X. Jiang, P. C. Wang, H. Y. Wang. "Height Estimation Algorithm Based on Visual Multi-Object Tracking", *Acta Electronica Sinica*, vol. 43, no. 3, (2015), pp. 591-596.
- [2] A. Criminisi, I. Reid, A. Zisserman. "Single View Metrology", *International Journal of Computer Vision*, vol. 40, no. 2, (2000), pp. 123-148. <https://doi.org/10.1023/A:1026598000963>
- [3] C. Benabdelkader, Y. Yacoob. "Statistical Body Height Estimation from a Single Image", *IEEE International Conference on Automatic Face & Gesture Recognition*, (2008), pp. 1-7. <https://doi.org/10.1109/AFGR.2008.4813453>
- [4] Q. L. Dong, Y. H. Wu, Z. Y. Hu. "Video-based Real-time Automatic Measurement for the Height", *Acta Automatica Sinica*, vol. 35, no. 2, (2009), pp. 137-144. <https://doi.org/10.3724/SP.J.1004.2009.00137>

- [5] J. Cai, R. Walker. “Height Estimation from Monocular Image Sequences Using Dynamic Programming with Explicit Occlusions”, *IET Computer Vision*, vol. 4, no. 3, (2010), pp. 149–161. <https://doi.org/10.1049/iet-cvi.2009.0063>
- [6] Y. P. Guan. “Unsupervised Human Height Estimation from a Single Image”, *Journal of Biomedical Science and Engineering*, vol. 2, no. 6, (2009), pp. 425–430. <https://doi.org/10.4236/jbise.2009.26061>
- [7] R. Q. Du, Y. Z. Gu, C. Zhang, Y. G. Wang. “Method of Pedestrian Height Measurement Based on Binocular Stereo Vision”, *Information Technology*, vol. 24, no. 1, (2016), pp. 91-95.
- [8] E. Jeges, I. Kispal, Z. Hornak. “Measuring Human Height Using Calibrated Cameras”, *Proceedings of the 2008 Conference on Human Systems Interactions*, (2008), pp. 755-760 <https://doi.org/10.1109/HSI.2008.4581536>
- [9] C. S. Zhou, Z. Shi. “Design of Height Measurement System Based on the Depth Image”, *Journal of Guilin University of Electronic Technology*, vol. 33, no. 3, (2013), pp. 214-217
- [10] Y. M. Mustafah, R. Noor, H. Hasbi, A.W. Azma. “Stereo Vision Images Processing for Real-time Object Distance and Size Measurement”, *International Conference on Computer and Communication Engineering*, (2012), pp. 659-663. <https://doi.org/10.1109/ICCCE.2012.6271270>
- [11] C. Madden, M. Piccardi. “Height Measurement as a Session-based Biometric for People Matching across Disjoint Camera Views”, *Image & Vision Computing New Zealand*, (2005), pp. 29.
- [12] Z. Zhang. “A Flexible New Technique for Camera Calibration”, *Transactions on Pattern Analysis and Machine Intelligence*, vol. 22, no. 11, (2000), pp. 1330-1334. <https://doi.org/10.1109/34.888718>
- [13] C. Stauffer, W. E. L. Grimson, “Adaptive Background Mixture Models for Real-time Tracking”, *Proceedings of IEEE Conference on Computer Vision and Pattern Recognition*, (1999), pp. 246-252. <https://doi.org/10.1109/CVPR.1999.784637>
- [14] C. Stauffer, W. E. L. Grimson. “Learning Patterns of Activity Using Real-time Tracking”, *IEEE Transactions on Pattern Analysis and Machine Intelligence*, vol. 22, no. 8, (2000), pp. 747-757. <https://doi.org/10.1109/34.868677>
- [15] Z. Zivkovic. “Improved Adaptive Gaussian Mixture Model for Background Subtraction”, *Proceedings of the 17th International Conference on Pattern Recognition*, (2004), pp. 28-31. <https://doi.org/10.1109/ICPR.2004.1333992>
- [16] T. Horprasert, D. Harwood, L. Davis. “A Statistical Approach for Real-time Robust Background Subtraction and Shadow Detection”, *IEEE ICCV Frame Rate Workshop*, (1999), pp. 1-19.
- [17] Bouguet J. “Camera Calibration Toolbox for Matlab[DB/OL]”. [http://www.vision.caltech.edu/bouguetj/calib\\_doc](http://www.vision.caltech.edu/bouguetj/calib_doc), (2010).
- [18] H. Bay, T. Tuytelaars, L. van Gool. “SURF: Speeded Up Robust Features”, *Computer Vision and Image Understanding*, vol. 110, no. 3, (2006), pp. 404-417. [https://doi.org/10.1007/11744023\\_32](https://doi.org/10.1007/11744023_32)
- [19] D. Lowe. “Distinctive Image Features from Scale-Invariant Keypoints”. *The International Journal of Computer Vision*, vol. 2, no. 60, (2004), pp. 91-110. <https://doi.org/10.1023/B:VISI.0000029664.99615.94>
- [20] G. Bradski, A. Kaehler. “Learning OpenCV: Computer Vision with the OpenCV”, O’Reilly Media, Inc, USA, (2008).

## 10 Authors

**Guangyi Yang**, he received his M.Sc. degree in Electronic Engineering from Wuhan University, China in 2008. He is currently an engineer in the School of Electronic Information, Wuhan University. His research interests involve in high frequency circuit and image processing, etc.

**Deshi Li**, he received the PhD degree in Computer Science from Wuhan University, China in 2001. Dr. Li is currently a professor and dean in the School of Electronic Information, Wuhan University. His research is involved in wireless sensor networks, networked robots, wireless communication, etc.

**Guobao Ru**, he received his B.S. degree in Electronic Engineering from Wuhan University, China in 1986. Dr. Ru is currently a professor in the School of Electronic Information, Wuhan University. His research is involved in wireless communication and machine vision, etc.

**Jiahua Cao**, he is currently studying for his B.S. degree at the school of Electronic Information in Wuhan University, China. His research interests include image processing and pattern recognition.

**Weizheng Jin**, he received his M.Sc. degree in Electronic Engineering from Wuhan University, China in 1991. He is currently an associate professor in the School of Electronic Information, Wuhan University. His research is involved in high frequency circuit and image processing, etc.

Article submitted 08 February 2018. Final acceptance 31 March 2018. Final version published as submitted by the authors.